IOP Publishing Journal of Physics: Condensed Matter
J. Phys.: Condens. Matter **30** (2018) 264001 (14pp) https://doi.org/10.1088/1361-648X/aac57a

Viral nanomechanics with a virtual atomic force microscope

María Aznar[1], Sergi Roca-Bonet[1,3] and David Reguera[1,2]

[1] Departament de Física de la Matèria Condensada, Universitat de Barcelona, Martí i Franquès 1, 08028 Barcelona, Spain
[2] University of Barcelona Institute of Complex Systems (UBICS), Martí i Franquès 1, 08028 Barcelona, Spain

E-mail: dreguera@ub.edu

Received 11 September 2017, revised 7 May 2018
Accepted for publication 15 May 2018
Published 5 June 2018

Abstract

One of the most important components of a virus is the protein shell or *capsid* that encloses its genetic material. The main role of the capsid is to protect the viral genome against external aggressions, facilitating its safe and efficient encapsulation and delivery. As a consequence, viral capsids have developed astonishing mechanical properties that are crucial for viral function. These remarkable properties have started to be unveiled in single-virus nanoindentation experiments, and are opening the door to the use of viral-derived artificial nanocages for promising bio- and nano-technological applications. However, the interpretation of nanoindentation experiments is often difficult, requiring the support of theoretical and simulation analysis. Here we present a 'Virtual AFM' (VAFM), a Brownian Dynamics simulation of a coarse-grained model of virus aimed to mimic the standard setup of atomic force microscopy (AFM) nanoindentation experiments. Despite the heavy level of coarse-graining, these simulations provide valuable information which is not accessible in experiments. Rather than focusing on a specific virus, the VAFM will be used to analyze how the mechanical response and breaking of viruses depend on different parameters controlling the effective interactions between capsid's structural units. In particular, we will discuss the influence of adsorption, the tip radius, and the rigidity and shape of the shell on its mechanical response.

Keywords: physical virology, coarse-grained simulations, atomic force microscopy, mechanical properties of viruses

(Some figures may appear in colour only in the online journal)

1. Introduction

Viruses are captivating nanoscale biological entities that in their simplest form are made by two essential components: a protein shell, also known as a *capsid*, and RNA or DNA as genetic material [1]. Despite this apparent simplicity, viruses are extremely efficient nanomachines capable of replicating with unparalleled efficiency in a wide variety of hosts and conditions. The most important role of the capsid is to protect the genetic material of the virus. During the extracellular phase viruses face large variations in environmental conditions that could induce extreme changes in temperature, pH, osmotic shocks related to a sudden alteration of salt concentration, or dehydration. In addition, the capsid of many double-stranded DNA viruses has to withstand up to tens of atmospheres of pressure built up during the packaging of the viral genome at high densities [2–7]. Moreover, extremophile viruses can live in extreme conditions of salinity, radiation or temperature [8]. Thus, it is very important that the capsid keeps its integrity under environmental changes and survives mechanical stresses during its life cycle. As a consequence viruses have developed amazing mechanical properties. Notable examples are bacteriophage ϕ29 that is capable of withstanding about

[3] Current address: Theoretical Soft-Matter and Biophysics, Institute of Complex Systems, Forschungszentrum Jülich, 52425 Jülich, Germany

50 atms of pressure inside [5, 7, 9]; or cowpea chlorotic mottle virus (CCMV) that tolerates broad pH ranges and deformations of more than 30% without breaking [10, 11].

In recent years, there has been a lot of interest in characterizing the mechanical properties of individual viruses [12]. These studies have been possible by the development and application of different single-molecule experimental techniques. In particular, optical tweezers have been crucial in measuring the forces associated to the packing of the genome [7]. But, arguably, the most important and popular tool has been the application of the atomic force microscope (AFM) to obtain the mechanical resistance and topography of individual capsids [12–17]. AFM nanoindentation experiments have determined different mechanical properties of viruses, including effective Young's modulus [13], breaking patterns and forces [18], fatigue [19] or even internal pressures [9].

AFM experiments are a very powerful tool to access mechanical information of viral capsids, but it is often very hard to get a good interpretation of the results and to relate this information to the biological characteristics of viruses. In this context, theoretical modeling and simulations are required to achieve a better understanding of experimental AFM results [20].

The goal of this article is precisely to introduce a 'Virtual AFM', i.e. a coarse-grained simulation mimicking the standard setup and experimental protocol of AFM nanoindentation experiments. Instead of placing the focus on the finest structural details of the nanoindentation of a specific virus, the aim is to provide a highly coarse-grained description, allowing to simulate large viruses at realistic timescales and with the advantage of being able to link the mechanical behavior to the essential physical ingredients of the interaction between capsid's structural units. With the VAFM one can get a better understanding of the mechanical response of viral capsids and how it will be influenced by changes in structure, loading or environmental conditions.

This article is organized as follows. Section 2 briefly summarizes the basics of AFM nanoindentation experiments in the study of viral capsids. Section 3 will be devoted to the description and implementation of the 'Virtual AFM', a Brownian Dynamics (BD) simulation mimicking the typical set up of single virus nanoindentation experiments. A detailed explanation of the main parameters of the interactions in the coarse-grained model and how they could be obtained from experiments and full-atom simulations is also provided. Next, we will show how the elastic response of viruses depends on different physical parameters of their effective interactions, including the bending rigidity of the shell, the adsorption to the substrate, the radius of the AFM tip or the capsid shape. Finally, our main findings are summarized in the conclusions.

2. AFM on viruses

The application of AFM has become a revolution in the study of the mechanical properties of viruses [15]. The AFM is a high-resolution imaging technique that allows an exquisite control of the height, position, and force in the study of individual viruses. With it, it is possible to acquire nanometric-resolution images, and also to perform a physical characterization of the rigidity of the sample. AFM can also be used in liquids, thus facilitating the study of biological samples in their natural environment.

AFM nanoindentation experiments are providing important information about the mechanical properties of viruses [12, 14, 16]. The use of this method on different viruses has revealed that they are mechanically robust structures with interesting elastic properties. As an example, bacteriophages have been found to have high effective Young's modulus, comparable to that of hard plastics [13]. The AFM is also being very helpful in order to infer the influence of the genetic material or other types of cargo [21] on the mechanical resistance and stability of capsids. Nanoindentation experiments comparing empty and full capsids have been performed on various viruses such as CCMV [10], Minute Virus of Mice [22], phages λ [23] and $\phi 29$ [9], adenovirus [24] or herpes simplex virus [25, 26]. In addition, the mechanical changes induced by the maturation process in viruses such as moloney murine leukemia virus [27], human immunodeficiency virus [28], HK97 [29] or T7 [30] have also been studied.

The basic set up of an AFM consists of a flat horizontal surface, that supports the sample and a small tip at the end of a cantilever which interacts with the sample. The position of the tip is controlled using a piezolectric device that can move the sample in all three directions by an applied electric voltage. In contact operation mode, when the tip touches the sample the cantilever suffers a deflection that is measured by a laser and a photodiode. From the deflection of the cantilever, one can get an accurate topographic image of the sample with nanometer resolution [15, 17]. The deflection can also be translated into a force with a resolution of about 10 pN, using the elastic constant of the cantilever, which can be determined using, for instance, Sader's method [31].

In a typical nanoindentation experiment, the sample is immobilized on a flat hard substrate. The cantilever is then lowered progressively, recording the force and deflection as a function of the vertical position of the tip [15]. A conventional experimental force curve as a function of the indentation is plotted in figure 1. For small indentations a linear force-response can be observed allowing the determination of the particle's effective spring constant from the slope. For larger indentations one can observe a non-linear behavior followed by the presence of strong discontinuities in the force-indentation curve that are often attributed to the mechanical failure of the capsid. The maximum indentation is the value of the indentation at which the first sudden drop in the force occurs, and the corresponding value of the force is identified with the 'breaking force'. These three parameters, namely the effective spring constant, the maximum indentation and the breaking force, are the standard output of nanoindentation experiments. But the challenge is to translate these simple measures into meaningful intrinsic mechanical properties and to identify what are the actual processes responsible for the different features observed in the force-indentation curves.

The mechanical information obtained by AFM experiments has traditionally been interpreted in the framework of continuum elasticity theory [32]. In the thin shell approximation [13, 17, 33], the elastic response of viral capsids depends on

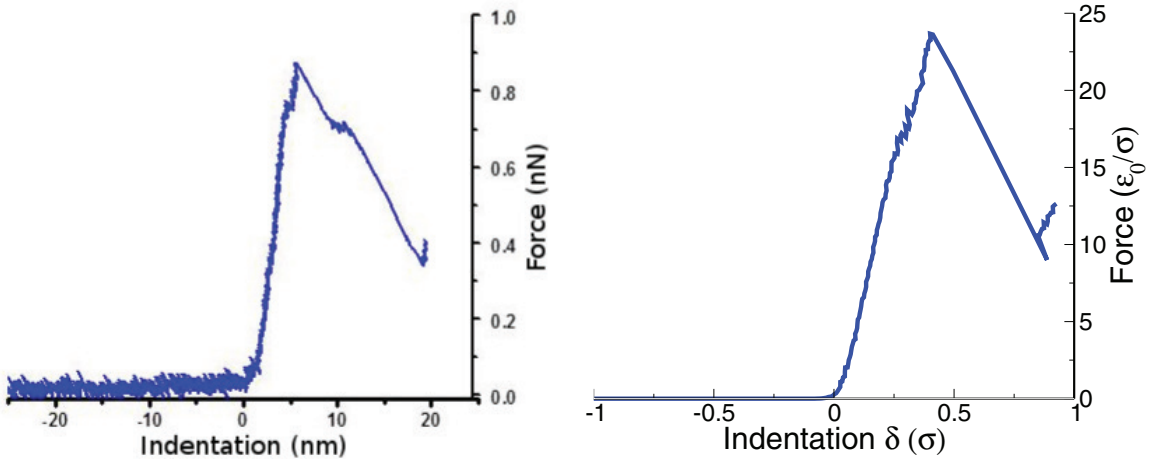

(a) (b)

Figure 1. (a) A typical force versus indentation curve obtained in a real AFM experiment for a bacteriophage T7 virus prohead indented along the 3-fold direction. The initial linear response ends abruptly by a sudden drop, in this case due to the fracture of the shell. Data courtesy of de Pablo's group. (b) A similar curve obtained in our simulations for a $T = 7$ shell. In the simulation, the sudden drop in the force is due to the breaking of the upper part of the virus. After the breaking event, the remaining part of the shell partially recovers its height, offering resistance to further indentation, as indicated by the subsequent increase in the force.

the competition between stretching and bending deformations and on the strength of the applied force (or depth of the applied indentation). One can distinguish two deformation regimes, corresponding to small and large indentation forces.

For small deformations the behavior of the force versus indentation is linear and reversible. In these conditions, the mechanical behavior of the cantilever can be approximated as an ideal spring whose elasticity is described by Hooke's law: $F = -k_c x$, where F is the restoring force, which is equal to the force of tip–sample interaction, k_c is the spring constant of the cantilever, and x is its deflection. The deformable sample can be considered like a spring in series with the cantilever. Using this approximation the effective elastic constant of the capsid is given by $k_{\text{cap}} = k_c \frac{S_g}{S_v - S_g}$, where S_g (nm V^{-1}) is the slope of the cantilever deflection on the non-deformable substrate and S_v (nm V^{-1}) the slope of the cantilever deflection on the virus. Thus, in the small deformations regime, k_{cap} is calculated from a linear fit of the force versus indentation curve. The spring constant of the virus k_{cap} is related to the effective 3D Young's modulus E as [17, 34]:

$$k_{\text{cap}} = \frac{2}{\sqrt{3(1-\mu^2)}} \frac{Eh^2}{R}, \tag{1}$$

where μ is the Poisson's ratio, R is the radius of the capsid, and h its thickness. The previous relation is exact for a thin spherical shell indented by a point force. For a thick shell, the same formula is used, replacing the prefactor $\frac{2}{\sqrt{3(1-\mu^2)}}$ by an effective coefficient which in most cases is close to 1. Alternatively, the spring constant can be rewritten in terms of the 2D Young's modulus $Y = Eh$ and the bending rigidity κ as [17, 35]

$$k_{\text{cap}} \sim \frac{\sqrt{\kappa Y}}{R}. \tag{2}$$

For indentations δ larger than the shell thickness, inverse buckling occurs [35]. In this regime, the force is no longer linear, but rather goes as $F \approx \sqrt{\delta}$. Inverse buckling is expected to happen when $\delta > h$ and when the force exceeds a critical value $F_{\text{inv}} \approx \kappa/R$. Applying even larger deformations eventually causes irreversible changes in the shell structure associated to bond ruptures.

Some of the approximations involved in thin shell theory can be removed by the use of finite elements (FE) simulations to solve the complex 3D continuum elasticity equations [10, 13, 36]. Using FE, it has been possible to analyze the effect of the thickness of the capsid, to extract phenomenologically the effective Young's modulus, and even to account for the effect of inhomogeneities using refined meshes constructed from atomic maps of viruses [37].

The continuum mechanics description works well as a first approximation and has provided very useful information about the elastic properties of viruses. However, a continuum description cannot capture the discrete nature of subunits forming the capsid, which is very important for a correct mechanical description of viruses [38]. As an example, AFM experiments on bacteriophage T7 show an anisotropic stiffness in its mechanical response [30] that cannot be described with a continuum theory. Therefore, accounting for the discrete and inhomogeneous nature of the capsid is crucial to properly understand its stability and mechanical response.

Different types of simulations, accounting for the discreteness of the capsid at diverse resolution levels, have been implemented in the literature. In particular, elastic network models have been used to study the buckling and deformation of viruses [35, 39, 40–45], but cannot easily account for breaking events. On the opposite extreme, full-atom or high-resolution, structure-based coarse-grained simulations of nanoindentation experiments are computationally very costly, specially when applied to large viruses [46–52]. That is the reason why we developed our 'Virtual AFM' described in the next section.

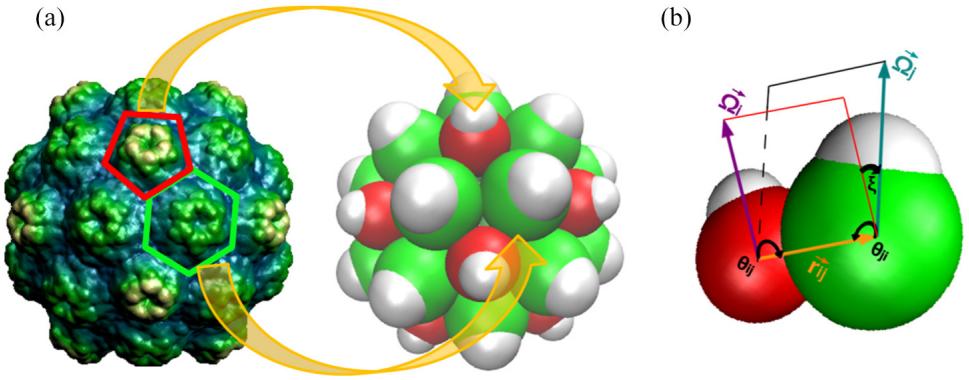

Figure 2. (a) Schematic representation of the coarse-grained modeling applied to the particular example of Turnip yellow mosaic virus (TMYV), a $T = 3$ virus. The left image is a surface view of the real capsid taken from VIPERdb [64]. Clusters of five (pentamers) or six (hexamers) coat proteins are replaced in the coarse-grained model (right figure) by effective spheres of different diameter. (b) Representation of a coarse-grained hexamer (green) and pentamer (red) used in the model, indicating the distance between their centers $\boldsymbol{r_{ij}}$ (orange), the orientation vectors $\vec{\Omega}_i$ (violet) and $\vec{\Omega}_j$ (blue) and the angles used in the interaction potential. A white sphere is overlapped on each capsomer just for representation purposes, to indicate its orientation.

Using a high level of coarse-graining one can reach longer timescales and perform efficient simulations while retaining the essential ingredients of the interaction between viral capsid subunits. Our model can be considered as an intermediate approach between continuum descriptions, that ignore the discrete nature of viral capsid proteins and cannot describe virus breaking, and structure-based coarse-grained simulations. Our goal is to provide a physical interpretation of viral mechanics at a discrete level, rather than aiming at capturing all the structural details involved in the deformation of a specific virus. With the VAFM one can visualize the dynamics of the capsid during the nanoindentation and correlate the features observed in the force-indentation curves with actual physical changes in the capsid. The model can be used to study the mechanical properties of viruses of arbitrarily large T-number and viruses whose structure is not known with atomic resolution, thus being potentially very useful to get information on the stability and resistance of any virus.

3. Virtual AFM

In order to reproduce nanoindentation experiments, we wanted to implement a simulation mimicking the typical AFM setup. Since we are interested in the response of the viral capsid and the dynamics of capsomers during the indentation process, we decided to use an algorithm based on BD simulations together with a coarse-grained model of a capsid that succesfully reproduces the structure and assembly of the lowest Caspar and Klug structures, as described in [53]. The model was specifically designed to study self-assembly, where a large number of capsomers and long time scales are required. At those conditions, the implementation of high-resolution coarse-grained models will be computationally very costly.

3.1. Coarse-grained model of a viral capsid

Viral self-assembly is a complicated and virus-specific process, which however shows some universal features. The most remarkable one is that, despite the differences in shape, size, sequence and conformation of coat proteins among different viruses, they end up adopting a common set of architectures. That suggests the existence of common traits in the effective interactions that underlay and justify the ubiquitous prevalence of icosahedral structures [54]. In icosahedral viruses, the viral coat proteins are distributed in morphological units, called capsomers, made of five ('pentamers') or six ('hexamers') proteins. Although the interactions between individual proteins are presumably very complex, the effective capsomer-capsomer interactions are expected to be simpler and more isotropic. Accordingly, our model [53] is coarse-grained at the level of capsomers, i.e. pentamers and hexamers, which are the basic structural units of a viral shell. These capsomers are represented as effective spheres of two different diameters: $\sigma_{\rm h}$ and $\sigma_{\rm p}$, reflecting the fact that hexamers and pentamers are made of a different number of proteins (six and five, respectively), see figure 2(a). The goal is thus not to provide structurally-detailed information of each individual coat protein but rather to capture the essential physical traits of the effective interactions between capsid's morphological units.

Three are the essential ingredients of the interactions required for a successful model of a capsid at this high level of coarse-graining. First, a short range repulsion is needed to mimic steric effects and prevent capsomer overlapping. Second, some kind of binding attraction is vital to keep the integrity of the capsid. Third, an orientational-dependent interaction is necessary to account for the anisotropy of capsomers and to form stable shell-structures rather than compact clusters. Accordingly, the interaction between capsomers is modeled using three contributions: a Mie-like, an angular, and a torsion potential, $V = V_{LJ} \cdot V_a \cdot V_{\rm tor}$. The Mie-like potential describes the binding and the excluded volume interaction between a pair of capsomers in terms of their relative distance, $\boldsymbol{r}_{ij}$. The expression used was

$$V_{LJ}(\boldsymbol{r}_{ij}) = \epsilon_{ij} \frac{n}{m-n} \left[\left(\frac{\sigma_{ij}}{r} \right)^m - \frac{m}{n} \left(\frac{\sigma_{ij}}{r} \right)^n \right], \qquad (3)$$

where σ_{ij} is the equilibrium distance corresponding to the minimum of the potential, r is the distance between capsomer

centers, ϵ_{ij} is the binding energy between capsomers, and m and n represent the power of the repulsive and attractive interaction terms, respectively, which set the range of the interaction potential.

The angular term of the potential is given by

$$V_a(\boldsymbol{r}_{ij}, \boldsymbol{\Omega}_i, \boldsymbol{\Omega}_j) = \exp\left(-\frac{(\theta_{ij}-\nu)^2}{2\alpha^2}\right)\exp\left(-\frac{(\theta_{ji}-\nu)^2}{2\alpha^2}\right), \tag{4}$$

where θ_{ij} is the angle between the vector $\boldsymbol{\Omega}_i$, describing the spatial orientation of the capsomer, and the vector $\boldsymbol{r}_{ij}$ (see figure 2(b)). The parameter ν is the preferred angle of interaction between proteins of different capsomers, which ultimately defines the size of the shell, and the parameter α controls the local bending stiffness, i.e. the energy cost required to bend two capsomers out of their preferred angle of interaction.

Finally, the last contribution to the potential is a torsion term included to account for the differences between the inner and outer surface of coat proteins, and to favor the formation of closed shells instead of connected surfaces with different concavity. This contribution is given by

$$V_{\text{tor}}(\boldsymbol{\Omega}_i, \boldsymbol{\Omega}_j) = \exp\left(-k_t\frac{(1-\cos\xi)}{2}\right), \tag{5}$$

where k_t is the torsion constant and ξ is the angle between the planes defined by vector $\boldsymbol{r}_{ij}$ and both orientation vectors (see figure 2(b)).

The model has been implemented in a BD simulation code using reduced units and a simple stochastic Euler's integration algorithm. In the standard version of this algorithm, the position of a particle at a time $t + \mathrm{d}t$ is given by

$$\boldsymbol{r}_i(t+\mathrm{d}t) = \boldsymbol{r}_i(t) + \frac{\boldsymbol{F}_i(t)\mathrm{d}t}{\eta} + \sqrt{2D\mathrm{d}t}\boldsymbol{\xi}, \tag{6}$$

where η is the friction coefficient, D is the diffusion coefficient, $\boldsymbol{F}_i(t)$ is the force on particle i, and $\boldsymbol{\xi}$ is a Gausssian distributed random number with zero mean and variance 1. For simplicity, we will use reduced units, normalizing all variables in terms of the diameter of hexamers $\sigma \equiv \sigma_h$, the diffusion coefficient of hexamers D, and the binding energy between hexamers $\epsilon_0 \equiv \epsilon_{\text{hh}}$. In these reduced units, the characteristic time is $\tau = \sigma^2/D$, and using Stokes–Einstein equation $D = \frac{k_B T}{\eta}$ to eliminate η, Euler's algorithm can be written in a simple way. More specifically, at time $t + \mathrm{d}t$, the positions $\mathbf{r}(t)$ and angles ($\theta(t)$ and $\phi(t)$) for each capsomer are given by

$$\mathbf{r}(t+\mathrm{d}t) = \mathbf{r}(t) + \frac{\mathrm{d}t}{T}\mathbf{F}_r(r) + \sqrt{2\mathrm{d}t}\boldsymbol{\xi}_r, \tag{7}$$

$$\theta(t+\mathrm{d}t) = \theta(t) + \frac{\mathrm{d}t}{2T}F_\theta(t) + \sqrt{\mathrm{d}t}\xi_\theta, \tag{8}$$

$$\phi(t+\mathrm{d}t) = \phi(t) + \frac{\mathrm{d}t}{2T}F_\phi(t) + \sqrt{\mathrm{d}t}\xi_\phi, \tag{9}$$

where T is the temperature in reduced units, $\mathrm{d}t$ is the time step (typically $\mathrm{d}t = 10^{-5}$), $\boldsymbol{\xi}_r$, ξ_θ, and ξ_ϕ are Gaussian distributed random numbers with zero mean a variance 1. The translational and orientational forces $\boldsymbol{F}_r(t)$, $F_\theta(t)$ and $F_\phi(t)$ are calculated from the interaction potential between capsomers. Further details and the explicit expressions of the forces can be found in [55]. It is worth emphasizing that the model can reproduce successfully the structure and assembly of the lowest T-number viral shells without requiring any additional constraints, templates or local rules.

Finally, a nice characteristic of the model is that the interaction parameters can be connected to elastic modulus in the continuum limit. In particular, the 2D Young's modulus is approximately given by [53]

$$Y = \frac{2\,nm}{\sqrt{3}}\frac{\epsilon_0}{\sigma^2}, \tag{10}$$

and the bending rigidity is

$$\kappa = \frac{3\sqrt{3}}{8}\frac{\epsilon_0}{\alpha^2}. \tag{11}$$

In the continuum limit, the elastic behavior of a thin shell depends ultimately on a single non-dimensional parameter, the Föppl–von Kármán (FvK) number $\gamma = \frac{YR^2}{\kappa}$, which is the ratio of the stretching and bending energies [43, 44, 56–59]. In terms of the parameters of our model, the FvK number becomes simply

$$\gamma = \frac{16\,nm}{9}\alpha^2\left(\frac{R}{\sigma}\right)^2. \tag{12}$$

3.2. Evaluation of model parameters

Another nice feature of the present coarse-grained model is that it only depends on very few parameters which have a clear and meaningful physical interpretation. In particular, the diameters σ_{h} and σ_{p} represent the effective size of an hexamer and a pentamer, respectively. They can be determined as the diameter of a sphere circumscribing the actual hexameric and pentameric capsomer of a real virus of interest (see figures 3(a) and (b)). The remaining parameters entering into the different interaction potential terms, can be determined for a specific virus either from experiments or atomistic simulations. More specifically, atomistic umbrella sampling molecular dynamics simulations can be used to the determine the potential of mean force (PMF) between two hexamers or pentamers [60]. Using the distance between the center of masses of two hexamers as reaction coordinate, it is possible to evaluate the atomistic PMF as a function of their separation. This can then be fitted to the Mie expression, equation (3), obtaining the values of m and n, controlling the range of the interaction and ϵ_{ij}, representing the minimum of the potential. This procedure has been implemented, for instance, to obtain the effective interaction potential between two CcmK2 hexamers in studies of carboxysome assembly [60]. Alternatively, the effective binding energy between capsomers can be obtained from assembly or calorimetry experiments [61] or estimated by calculating the association energies in the atomistic equilibrium structure, considering the sum of energies due to desolvation, electrostatic, and van der Waals interactions between all atoms of the interacting subunits [62].

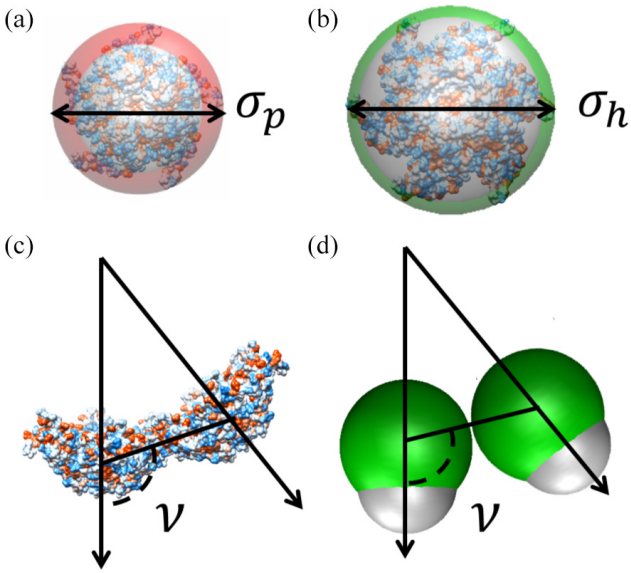

Figure 3. Surface representation of the atomic structure of a pentamer (a) and an hexamer (b) of TMYV. The size of the corresponding coarse-grained pentamer, σ_p, (in red) and hexamer, σ_h, (in green) is determined by the diameter of the sphere circumscribing the actual pentamer and hexamer, respectively. (c) The parameter ν in the model describes the preferred angle of interaction between capsomers and in most cases can be approximated by the angle between two neighbor capsomers in the native structure. The image (c) shows the value of ν obtained from two hexamers in the native structure of TMYV, and (d) is the corresponding representation in the coarse-grained model.

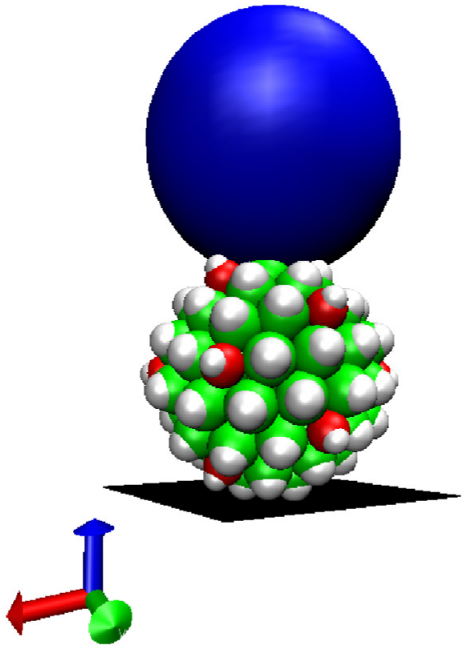

Figure 4. Snapshot of a $T = 7$ coarse-grained empty shell indented along the 2-fold direction. The blue sphere represents the AFM tip. The viral capsid is modeled at the level of capsomers, where hexamers and pentamers are represented by green and red spheres, respectively. The black rectangle illustrates the hard substrate.

The parameter ν describes the optimal angle of interaction between two capsomers. It can be approximated by the actual angle between hexamers in the native structure (see figure 3(c)) or even estimated for each T-number shell from a simple geometrical relation [53] $\cos(\nu) = -\sigma/(2R)$, where R is the radius of the capsid. Alternatively, it could be evaluated from the PMF in a full-atom simulation of two capsomers in contact for different relative orientations. The orientation corresponding to the minimum of the PMF will directly determine the value of ν. These simulations will be also useful to evaluate the local bending rigidity α, accounting for the energy required to bend the contact between two capsomers out of the preferential angle of interaction. The same simulations can also be used to determine the parameter k_t of the torsion potential, by getting the PMF of two hexamers in contact using the torsion angle as reaction coordinate.

Hence, by following this protocol one could get an accurate coarse-grained interaction potential between capsomers. With it, one could provide a nearly quantitatively accurate description of nanoindentation experiments of a specific virus of interest. The VAFM thus represents a sort of multiscale approach to simulate the mechanical properties of viruses, where the precise values of the parameters of the effective interactions can be determined from all atom simulations involving just two capsomers, and the global response of the capsid can be simulated at larger length and time scales using a very simple and efficient coarse-grained model. However, instead of pursuing this route for a particular virus, our aim in this work is to perform a more physical study and to explore how the mechanical response and some of the peculiar features observed in AFM nanoindentation experiments depend on the global physical parameters and energetic contributions describing the effective interactions.

To that end, we will focus on a specific T-number shell, choosing reasonable values of the parameters and working in reduced units (instead of real units) so that the results can be applied to a wide class of viruses. More specifically, we will study a generic $T = 7$ shell (representative, for instance, of bacteriophage λ, P22 or T7), fixing a reasonable value of the binding energy, namely $\epsilon_{hh} = 20k_BT$, which is a characteristic value of the association energies between capsomers obtained from atomic structures in [62]. For this choice, the reduced temperature becomes $T = 0.05$. All our simulations have been performed with $m = 12$ and $n = 6$, i.e. the standard parameters of a Lennard-Jones potential, since those values have been found to reproduce efficiently the assembly of the smallest Caspar and Klug structures [53]. For a $T = 7$ shell, the appropriate preferred angle between capsomers can be approximated by $\nu = 1.796$, corresponding to the lowest energy structure in [53]. We have set a value for the torsion constant of $k_t = 1.5$, but its precise value does not affect the mechanical response of the shell significantly.

3.3. Simulation set-up

The VAFM is a simulation that emulates the nanoindentation process of virus by an AFM, i.e. it simulates the lowering of a spherical tip attached to a microcantilever which exerts a force on a sample, in this case, an empty viral nanocage. The simulation setup is shown in figure 4. In the simulations we have added a rigid surface at a position $z = 0$, representing the

substrate; the tip of a cantilever at the top, modeled as a sphere which can only move in the z direction, and a preformed capsid between them mimicking the experimental situation. The capsomers, depicted by the red and green spheres in figure 4, interact pairwise through the coarse-grained potential described earlier. They also interact with the tip and with the substrate.

The interaction between capsomers and the sphere of radius R_t representing the AFM tip (depicted in figure 4 by a blue sphere) is modeled by the following purely repulsive harmonic potential

$$V_c = \frac{1}{2}k_{\text{rep}}\left(r_{ic} - (R_t + \sigma_i/2)\right)^2 \quad \text{if} \quad r_{ic} < R_t + \sigma_i/2, \qquad (13)$$

where k_{rep} is an effective repulsive spring constant, r_{ic} the distance between the center of the cantilever and capsomer i, and σ_i is σ_p or σ_h for a pentamer or a hexamer, respectively.

To mimic the deflection of the cantilever caused by the interaction with the capsid, its z-position is updated using the following overdamped Euler equation

$$z_c = \mathrm{d}t\frac{D_c}{k_{\text{B}}T}(F_c - k_c(z_c - h)) + \xi\sqrt{2D_c\mathrm{d}t}, \qquad (14)$$

where $\mathrm{d}t = 10^{-5}$ is the time step used in the simulations, $F_c = -\sum_i k_{\text{rep}}\left(r_{ic} - (R_t + \sigma/2)\right)$ is the total force on the cantilever due to the interaction with all capsomers, k_c is the spring constant of the cantilever, D_c is its diffusion coefficient, and ξ is a Gaussian noise with zero mean and variance 1.

Finally, the substrate (figure 4, black surface) is modelled as a flat rigid surface. To account for potential effects of adsorption with the substrate, as often occurs in experiments, a binding energy of adsorption E_{ads} is considered. This adsorption contribution is described by the interaction potential

$$V_{\text{sub}}(r) = E_{\text{ads}}\left[\left(\frac{\sigma_i/2}{|z|}\right)^{12} - 2\left(\frac{\sigma_i/2}{|z|}\right)^{6}\right], \qquad (15)$$

where $\sigma_i/2$ is the radius of capsomer i and $|z|$ is the distance between capsomer i and the substrate.

In the initial configuration, the empty capsid is placed slightly above the surface and the positions and orientations of all capsomers correspond to the optimal values for the parameters and T-number used. To prevent rotation and sliding in the simulations, the position of some capsomers is fixed, depending on the orientation of the virus. Specifically, for indentations along the 5-fold symmetry we have fixed four pentamers: the two pentamers located on the z-axis can only move in the z direction and another two pentamers having initially $y = 0$, cannot move in the y-direction. For indentations along the 3-fold, two pentamers have x, y fixed and can only move along z; and another two pentamers are fixed at $x = 0$.

In all simulations some parameters have been fixed, unless stated otherwise: the radius of the tip was set to $R_t = 3\sigma$ and the spring constant of the cantilever to $k_c = 40\epsilon_0/\sigma^2$. For a typical capsomer size of $\sigma \sim 10$ nm and binding interaction $\epsilon_0 \sim 20k_{\text{B}}T$, this would correspond to a tip radius of $R_{\text{t}} = 30$ nm and cantilever spring constant $k_c \sim 0.03$ N m^{-1}, which are experimentally reasonable values. Using the Stokes–Einstein equation to estimate the diffusion coefficient of this typical capsomer size, we get a a characteristic time $\tau = \sigma^2/D \sim 2.3$ μs. The strength of the tip-capsomer repulsion was set to $k_{\text{rep}} = 80\epsilon_0/\sigma^2$, but the specific value of this parameter is not relevant, since the same results were reproduced for $k_{\text{rep}} = 160\epsilon_0/\sigma^2$.

As in experiments, the simulation procedure involves the progressive lowering of the tip. In our simulations, the z position of the cantilever is initially set to a value above the shell and it is lowered at steps of 0.005σ. We lower the tip typically after 10^6 steps, measuring the average force on the cantilever sampled every 100 steps. The simulation runs for a total of 5×10^8 steps corresponding to a total indentation of 2.5σ. For a typical capsomer size of $\sigma \sim 10$ nm, the indentation speed in real units will correspond to 2 μm s^{-1}, which will be a relatively fast indentation. In some simulations, the retraction of the tip is also simulated, to check the reversibility, using the same number of steps and height increments.

With the 'Virtual AFM' it is possible to study the mechanical properties of different capsid structures. Our high-level of coarse-graining makes this model particularly suitable to analyze the nanoindenation of viruses whose detailed atomic structure is not known or of large viruses. As an example, figure 5 shows a snapshot of a simulation and a typical nanoindentation curve obtained with our VAFM for two large viral shells: a $T = 13$ shell, resembling the external layer of infectious bursal disease virus, and a $T = 25$ shell mimicking the nanoindentation of adenovirus. To our knowledge, those large shells have not being simulated using full-atomistic or structure-based coarse-grained simulations, since the number of residues involved would make them computationally very expensive.

For the sake of simplicity, in this work, we will focus on an empty $T = 7$ viral shell as a particular example. The $T = 7$ capsid is a chiral structure that can have two different chiralities: leavo and dextro [63]. In our simulations we have used a $T = 7$ leavo structure, since this chirality seems to be the most abundant for $T = 7$ viruses of known structure [64]. We have also performed simulations for a $T = 7$ dextro shell, finding no significant differences in the results.

3.4. Nanoindentation curves

Figure 6 shows three repetitions of a typical nanoindentation curve obtained from simulations of a 5-fold oriented $T = 7$ capsid including also the retraction of the tip. As in experiments, from the force F versus z curves we calculate the indentation as $\delta = -z_c - F/k_c + z_0$, where z_c is the position of the cantilever. The indentation curves are also shifted in z by a distance z_0 in such a way that the tip-sample contact starts at $\delta = 0$.

For small indentations, the F versus δ curves show a linear and reversible behavior corresponding to elastic response. At large indentations the linear regime ends up by an abrupt decline of the force, corresponding in this case to the sinking of the top pentamer, that gets inside the capsid, leaving a small hole behind. A second abrupt drop in the force is observed

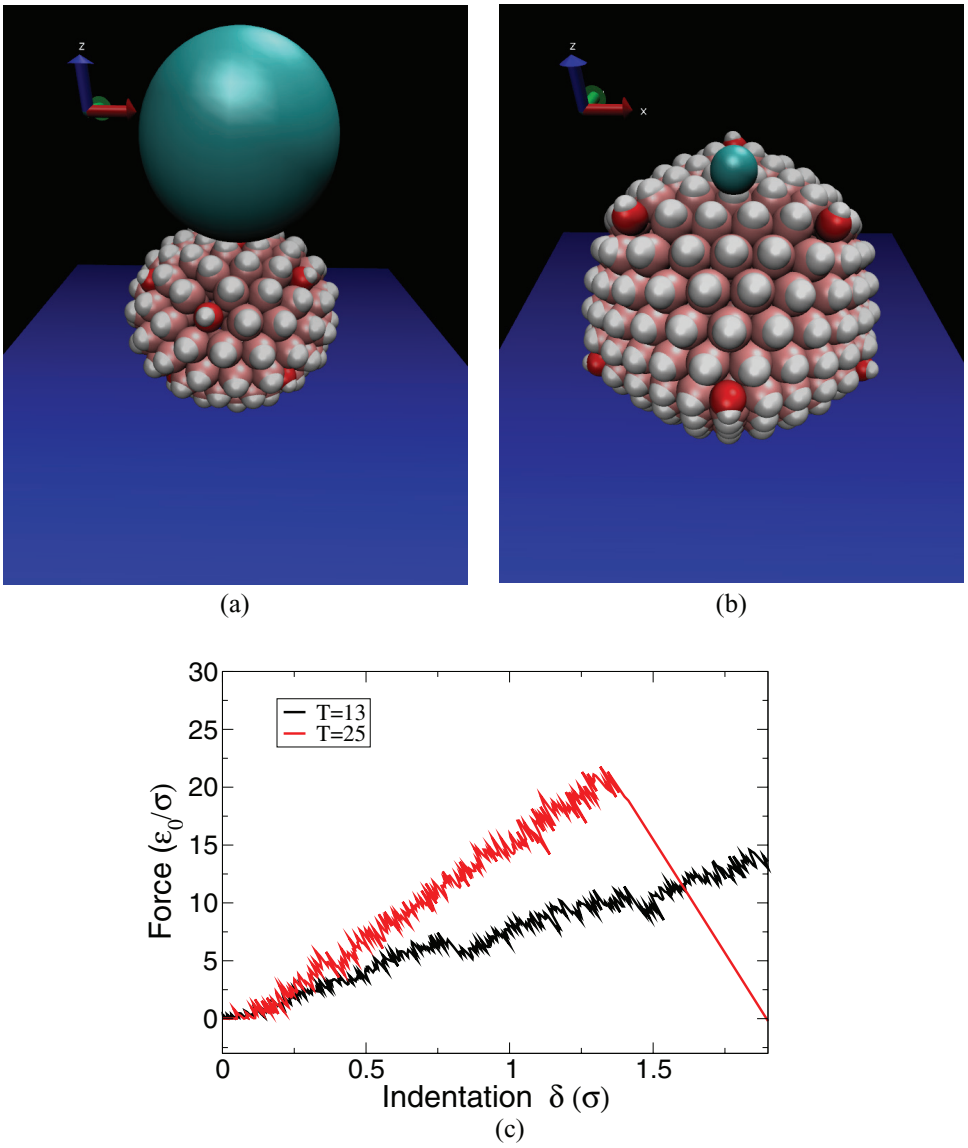

Figure 5. Snapshot of (a) a $T = 13$ and (b) a $T = 25$ empty shell indented with the VAFM. (c) Force versus indentation curves obtained in both cases. For the $T = 13$ shell, the parameters were $\nu = 1.796$, $\alpha = 0.2$, $R_t = 3$, and $E_{ads} = 0.1$. For the $T = 25$ shell, we used $\nu = 1.695$, $\alpha = 0.3$, $R_t = 1$ and $E_{ads} = 0.1$.

when the tip breaks the upper part of the capsid generating a large hole. This cracking of the capsid is not reversible, as shown by the different routes followed by the retraction curves of the tip. The final structure after retraction sometimes is partially healed as shown in the inset figure of a structure missing one pentamer with a small hole and pentamers and hexamers reorganized.

Figure 7 shows similar nanoindentation curves obtained when a 'soft' virus, i.e. one with a relatively low bending stiffness, is indented along its 3-fold axis of symmetry. The indentation curves show an initial linear regime followed by an increase in the slope ended by an abrupt drop in the force which in this case is not associated to the breaking of the shell, but rather to its flattening on top of the substrate, as will be discussed in more detail later on. The critical force and indentation associated with the sudden drop of the curves change in different repetitions of the same simulation. This is indicative of the stochastic, temperature-activated nature of this phenomenon.

It is worth emphasizing that the indentation curves obtained using our 'Virtual AFM' are remarkably and qualitatively nearly identical to the experimental curves measured with the real AFM, as illustrated in the comparison between figures 1(a) and (b).

4. Results

As mentioned before, one of the potential uses of the VAFM would be to focus on a specific virus of interest and try to reproduce quantitatively experimental nanoindentation curves by tuning properly the values of the effective interaction parameters. Rather than following this approach, we have opted in the present work to use the VAFM to analyze in global physical terms how the mechanical response of a viral capsid measured in a nanoindentation experiment depends on the physical characteristics of the interaction. In particular,

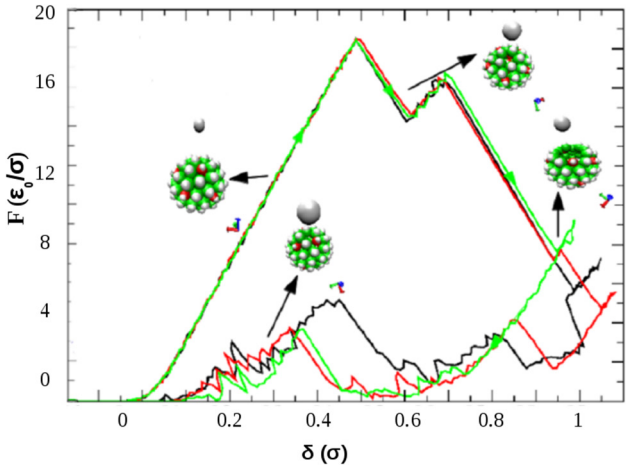

Figure 6. Force versus indentation in the 5-fold orientation for a $T = 7$ shell with all capsomers having the same size, for a rigid shell with $\alpha = 0.1$, $\nu = 1.796$, $k_c = 40$, $k_{\text{repul}} = 80$, $E_{\text{ads}} = 0.1$, and $T = 0.05$.

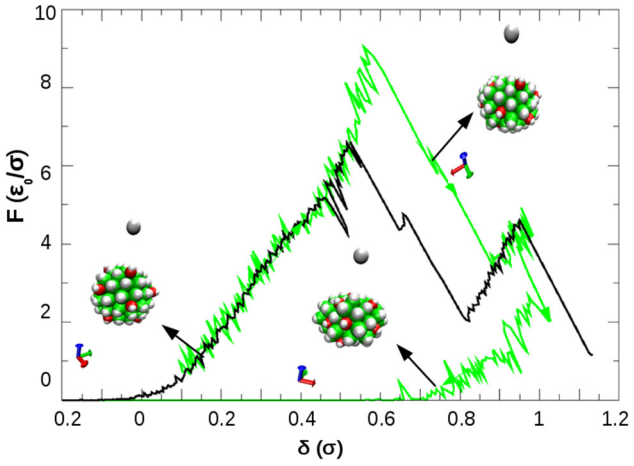

Figure 7. Two repetitions of a force versus indentation curve for indentation along the 3-fold direction of a relatively soft $T = 7$ shell with $\alpha = 1.0$, $E_{\text{ads}} = 0.1$, and all capsomers having the same size.

we analyze the influence on the mechanical response of different parameters, such as the bending stiffness, related to the parameter α, the radius of the tip, the adsorption energy of the substrate E_{ads}, and the geometry of the indentation. The results are briefly summarized in the following subsections.

4.1. Influence of the bending stiffness

Figure 8 shows the influence of the bending rigidity on the indentation along the 5-fold orientation of a $T = 7$ shell with one type of capsomer. The bending rigidity κ of the shell is dictated by the parameter α through equation (11). As α increases, the bending rigidity decreases and the capsid becomes softer, tolerating larger indentations. For $\alpha \in [0.1, 0.5]$ the shape of the shell is spherical and the effective spring constant, obtained from the slope of a linear fit for small indentations, decays as $k_{\text{cap}} \sim \sqrt{\kappa} \sim 1/\alpha$, as predicted by thin-shell theory [17, 35]. The sudden drop in the force curves for $\alpha = 0.1$ and $\alpha = 0.2$ corresponds to a breaking event, associated with the opening

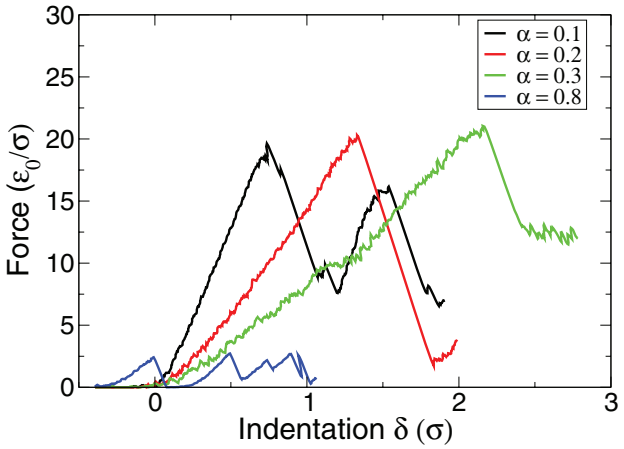

Figure 8. Force versus indentation curve in the 5-fold orientation for a $T = 7$ structure having all capsomers of the same size, for $E_{\text{ads}} = 0.1$ and different values of the parameter α that controls the bending rigidity of the shell.

of a hole in the upper part of the capsid. However, for $\alpha = 0.3$ the capsid is very soft, and resists large indentations (of up to 75% of its radius), until its final collapse into a pancake-like shell. For $\alpha > 0.3$, the shell becomes progressively more faceted. This faceting is noticeable by an increase in its 5-fold height, signalled in the figure by the shifting in the contact point towards negative values. For $\alpha > 0.6$ the shell undergoes a buckling transition [43], as indicated by the change in height. The several drops observed in the measured force are due to a progressive faceting or flattening of the shell on top of the substrate rather than to an actual breaking event (which is unlikely because the structure is very soft).

An important conclusion of this study is that the effective spring constant measured by AFM is not only determined by the strength and range of the binding interactions (which in this case are kept constant) but also by the bending cost to drive the capsomers away from their preferred angle of interaction. Thus, the Young's modulus is not the only elastic constant determining the effective spring constant of a virus. This aspect, qualitatively captured by equation (2), is often overlooked in the interpretation of experiments.

4.2. Influence of the adsorption energy E_{ads}

One recurrent question concerning nanoindentation experiments is the influence of the substrate on the measured mechanical properties of viruses. We have analyzed the influence of the adsorption strength with the substrate on the indentation curves for capsids of different bending rigidity. Figure 9 shows the results for a relatively rigid shell with $\alpha = 0.1$. At small values of the adsorption energy, $E_{\text{ads}} < 1$, the capsid keeps its nominal height and the slope of the indentation curves is insensitive to E_{ads}. However the maximum value of the indentation before the first drop in the force occurs goes down as the adsorption gets stronger. The drop corresponds in this case to the flattening of the bottom part of the virus induced by the applied force.

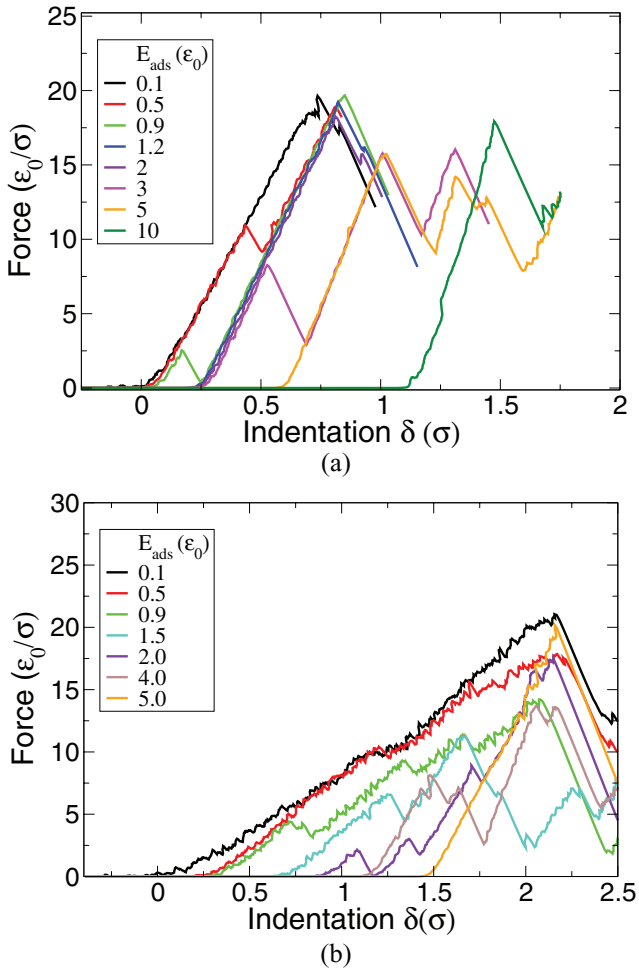

Figure 9. Force versus indentation curves for indentations along the 5-fold direction of a $T = 7$ structure using all capsomers of the same size for different values of the adsorption energy E_{ads} for (a) a rigid shell with $\alpha = 0.1$ and (b) a softer shell with $\alpha = 0.3$.

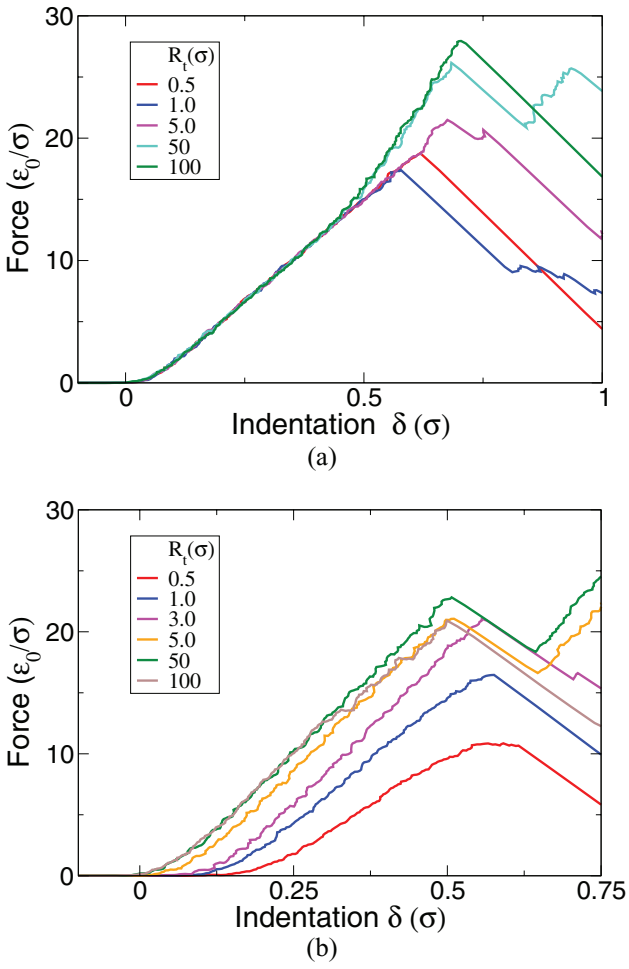

Figure 10. Force versus indentation curve for a $T = 7$ shell using all capsomers of the same size for $E_{ads} = 1.0$ and different tip radius R_t indented along (a) the 5-fold direction and (b) the 3-fold direction.

For $1 < E_{ads} < 4$, the bottom pentamer and the five surrounding hexamers are initially adsorbed on the substrate leading to a well-defined initial height of the capsid which is smaller than the nominal height (reflected in figure 9 by a shift of the contact point between the tip and the sample).

At very large adsorptions, $E_{ads} > 4$, the strong adsorption eventually flattens and breaks the bottom part of the shell, which stands on the substrate by an adsorbed ring of hexamers, exhibiting a well defined reduced height. As E_{ads} further increases, the height of the supported dome gets down at discrete steps (see the dark green curve in figure 9 for $E_{ads} = 10$), corresponding to different number of adsorbed capsomers at the adsorption rim. Remarkably, the strongly adsorbed shell which has a broken bottom still exhibits almost the same spring constant as the intact shell.

For $\alpha = 0.3$, corresponding to softer shells with smaller bending rigidity, there is a wide variability of adsorption heights, instead of the discrete set observed for $\alpha = 0.1$. This behavior has been recently reported experimentally and used to estimate the bending rigidity of Brome mosaic virus [65]. If the adsorption energy is very weak, the indentation curve shows a smaller slope and an inflection or steps in the middle due to the progressive flattening of the bottom part or the lateral faces induced by the force. As E_{ads} increases, the shell shows different apparent heights, corresponding to different levels of adsorption, but the same initial spring constant. For $E_{ads} > 4$, the shell is strongly adsorbed on the substrate, leading to a partial reorganization of the capsomers and a higher spring constant. Remarkably, despite the strong adsorption, no breaking of the bottom part of the shell occurs even at $E_{ads} = 10$.

To summarize the effects of the substrate, the slope is nearly the same in all curves, showing that reasonable adsorption with the substrate has no significant influence on the stiffness measured in the AFM [65]. However, the apparent heights, breaking forces and critical indentations depend on the adsorption strength and typically get smaller as the adsorption gets larger.

4.3. Influence of the tip radius

Another interesting aspect to explore is the potential influence of the tip radius on the nanoindentation curves. Figure 10 shows the curves obtained using different tip radius for

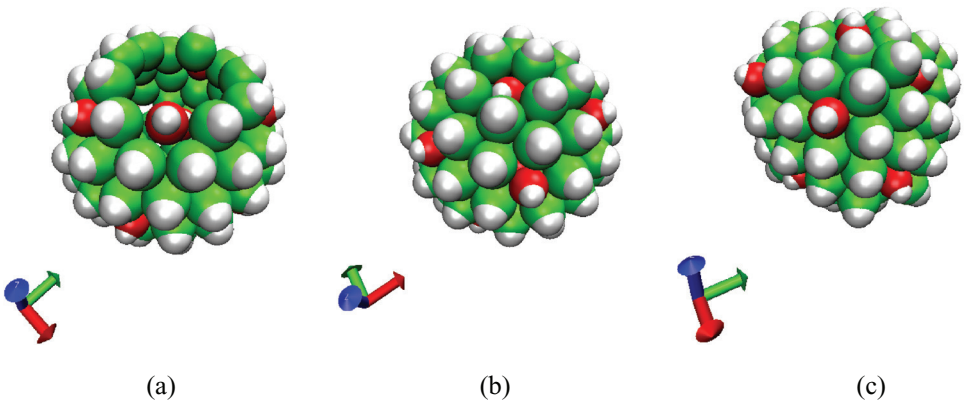

Figure 11. Snapshots taken just after a sudden drop in the force curve corresponding to (a) an example of breaking for large indentations along the 3-fold direction and two examples of buckling: (b) in the 5-fold direction, due to the entrance of the top pentamer and (c) in the 3-fold direction, associated to the faceting of the shell.

nanoindentations along the 5-fold and 3-fold directions. Remarkably, for indentations along the 5-fold axis (see figure 10(a)) the well defined contact of the tip with the top pentamer makes that all curves coincide having the same slope. The slope only changes for large indentations for $R_t > 5$, when the tip radius is large enough to press on more than one capsomer at a time. Contrarily, for indentations along the 3-fold axis of symmetry (see figure 10(b)), the tip is placed in the space between three hexamers, and the contact height depends on the tip size, as indicated by the shift of initial contact points. In addition, the slopes are different and increase continuously with the tip radius up to converging to a constant value for very large, essentially flat, tips. Therefore, the results suggest that the radius of the tip leads to changes in the measured height and spring constant whenever it permits the contact with a larger area of the capsid.

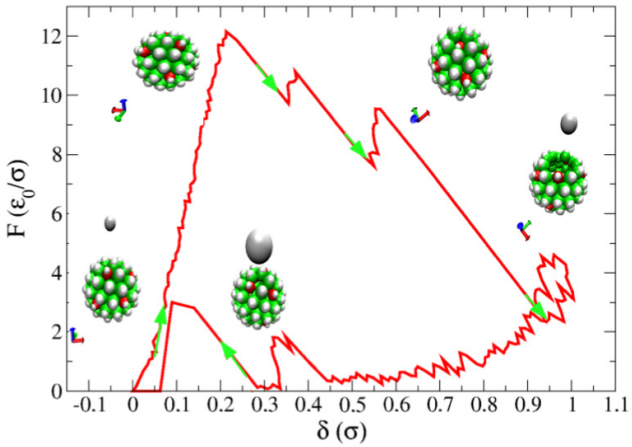

Figure 12. Force on the cantilever versus indentation in the 5-fold direction for a $T = 7$ shell using $E_{hp} = 0.7$, showing different examples of the mechanism responsible for the sudden drops in the force.

4.4. Buckling and breaking of viral capsid

One of the most representative characteristics of both experimental and simulated indentation curves are abrupt drops in the force, that occur after the initial linear regime. These force drops have been traditionally attributed to capsid breaking, see figure 1(a). However, in the simulations we see that many different physical phenomena can happen with the same signature corresponding to a drop in the force. The advantage of the simulations is that one can correlate the observed drops in the force with snapshots obtained from the simulations. In that way, we have observed that sudden drops in the force correspond, very often in an indistinguishable way, to breaking, buckling, rotation and/or sliding. Rotation and sliding are the most common cause of sudden drops in the force when the capsid is not properly immobilized on the substrate. When rotation and sliding are prevented, one could still observe breaking, buckling, and reorganization of capsomers, see figure 11.

It is important to distinguish between breaking and buckling events. *Breaking* is defined as the disruption of the capsid involving rupture of intercapsomer bonds. This is typically an irreversible phenomenon that is associated with the presence of a crack or hole in the capsid (see figure 11(a)), as can be observed also in AFM experiments. Breaking is important for the life cycle of virus, since it will expose the genome. In nanotechnological applications it is indispensable to prevent the unwanted breaking of the shell for nanoencapsulation. In a *buckling* process there is a collective change in the position of several capsomers, leading to a faceting of the structure, without cracks, see figure 11(c). If the indentation stops just after a buckling event and the tip is retracted we could observe very often that this buckling is reversible.

The goal of this section is to characterize a bit better these phenomena and how they depend on different factors such as the bending stiffness of the shell. This information is potentially useful to tune the mechanical resistance of a capsid for different applications or to promote its disruption.

A good example of different drops in the force under indentation is plotted in figure 12, corresponding to a relatively rigid $T = 7$ capsid indented along the 5-fold direction. This figure shows first a buckling process. The second drop corresponds to the collapse of the bottom pentamer, that adopts the same z-position as the hexamers around it and the third drop is when the structure actually breaks.

In experimental force curves the force drops are identical to the ones observed in the simulations, but the mechanism involved in the drop is unknown in most cases. It is usual to interpret always a drop in the force as a breaking event. But with the help of our simulation one can see that this is not always correct, and that the mechanism depends on the elastic characteristic of the capsid. When the bending rigidity of the shell is large, the shell is more fragile, and breaking events are usually the most probable cause of force drops. Buckling appears normally for low values of bending stiffness, corresponding to soft shells that deform easily, preventing rupture.

4.5. Polyhedral versus spherical shells

Many viruses, such as bacteriophage T7, change their shape from spherical to polyhedral during the maturation of their capsids [66]. This change in viral shape is present in the maturation of others viruses such as λ or HK97 [29, 67] and it is indispensable to become infective.

The change in shape might alter the mechanical response of the shell and could bring some mechanical advantages [38]. Previous works on viruses like λ and HK97, which suffer a transition between spherical and polyhedral shapes during their maturation, show mechanical changes. In particular, λ mature virion is more resistant than its prohead [14, 29] or HK97 virion is stiffer than its prohead, but the prohead tolerates larger deformations [29].

In this section we compare the mechanical response of our model $T = 7$ shell in its spherical and polyhedral shapes. Using the 'Virtual AFM' it is possible to obtain qualitative information about the mechanical changes associated to a shape change, as the one occurring in viruses upon maturation.

In our study, the change in shape was obtained by changing the parameter α related to the bending stiffness [53]. In particular, it was found in [53] that $T = 7$ structures with one type of subunit exhibit a transition between a spherical shape and a polyhedral shape at $\alpha \approx 0.6$. The structure become progressively more and more faceted as α is further increased. We have chosen the values of $\alpha = 0.1$ to represent the spherical prohead and $\alpha = 1.0$ for the mature capsid because for this value the structure is noticeable faceted, but stable enough to sustain AFM indentations.

As an example, we will analyze the case of bacteriophage T7 with one type of morphological subunit. A value of the interaction between hexamers and pentamers of $E_{\rm hp} = 1.4E_{\rm hh}$ was chosen to reproduce the relative strength of the hexamer–hexamer and hexamer–pentamer contact energies reported from the atomic structure in [30, 68].

Figure 13 shows the force versus indentation curves obtained for the model 'prohead' (circles) and 'mature capsid' (triangles) along the 2-fold, 3-fold and 5-fold symmetry axes. In general the spherical shape, for all folds, is stiffer than the polyhedral shape, due to its higher bending rigidity.

We have calculated the spring constants for both shapes and observed a change in their relative ordering. Specifically, we obtained $k_3^{sp} = 55.6, k_2^{sp} = 48.2, k_5^{sp} = 34.2 \pm 0.5\ \epsilon_0/\sigma_0^2$. Thus, the 3-fold is the stiffest and the 5-fold is the softest. In contrast, for the polyhedral shape we obtained $k_2^{ico} = 11.6, k_3^{ico} = 9.9, k_5^{ico} = 5.8 \pm 0.5\ \epsilon_0/\sigma_0^2$, and thus the softest orientation is the 5-fold, and the stiffer is the 2-fold, yielding an order of constants $k_2 > k_3 > k_5$.

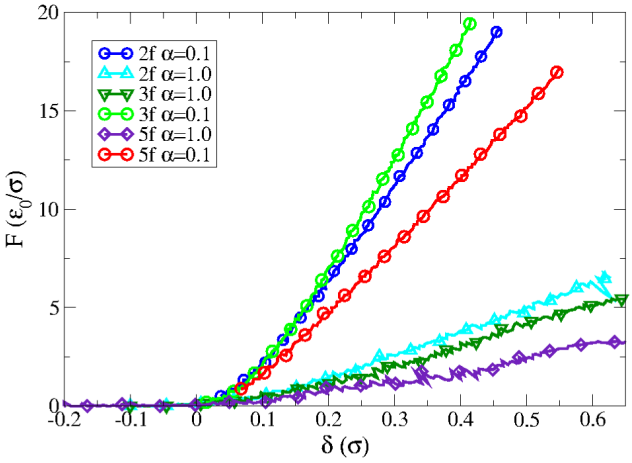

Figure 13. Indentation curves for a $T = 7$ capsid for $k_c = 40$, $k_{\rm repul} = 80$, $E_{\rm hp} = 1.4$ and $\sigma_p = \sigma_h$ for different orientations of a spherical capsid with $\alpha = 0.1$ (circles) and for a polyhedral shell with $\alpha = 1.0$ (triangles).

The spring constants obtained in experiments are similar for the prohead and virion in all symmetry axes, contrarily to our simulations. This discrepancy is mainly due to the fact that the increase in α required to obtain the polyhedral shape also modifies significantly the global stiffness of the shell. Thus, in its present form, our model cannot capture realistically the complicated changes associated to viral maturation. However, the order of the spring constant for our polyhedral shell is the same as that found in nanoindentation experiments for the mature *T*7 capsid [30]. Remarkably, the anisotropic elasticity obtained from AFM indentation experiments of T7 viral capsids does not follow the anisotropy expected from continuum homogenous models [23]. Whereas the experimental results show the spring constant of T7 capsids for each icosahedral symmetry axis as $k_{5c} < k_{3c} < k_{2c}$, FEM simulations of the stiffness performed in thin shell continuum models establishes $k_5 < k_2 < k_3$ [30]. In addition, FE simulations of a thin or thick icosahedral shell with the same dimensions as T7 also predict an incorrect order of the spring constants. Remarkably, the results obtained with our VAFM reproduce the same order of the effective spring constants found in the experiments (i.e. $k_{5c} < k_{3c} < k_{2c}$). This suggests that the distinct stiffnesses for the different orientations found in the T7 capsid are associated to the discrete nature of its structural components and to their particular arrangement in the final structure.

5. Conclusions

In this article we have presented the implementation of a 'Virtual AFM', a BD simulation using a coarse-grained model for a viral capsid, designed to mimic the standard setup of AFM nanoindentation experiments. This 'Virtual AFM' is a very useful tool to investigate the mechanical properties of viruses, and how they change with the relevant physical

parameters. With this tool it is also possible to interpret real experiments, providing a simple way to account for the influence of the discrete structure of the capsid, and obtaining very useful information about the physical ingredients involved in the mechanical response of viral capsids.

Our 'Virtual AFM' has been already useful to interpret experiments performed on bacteriophage T7 [30]. The simulations explain the unusual anisotropic stiffness found in these experiments, and reproduce qualitatively the experimental results. We have also analyzed how the measured stiffness depends on different physical parameters, and on the shape of the virus. In particular, we have shown that the measured spring constant not only depends on the Young's modulus of the shell but also on the local bending rigidity between subunits. We have also analyzed the influence of the adsorption with the substrate on the elastic response of a virus. Our findings suggest that the effective spring constant of the virus is almost insensitive to the substrate, but the virus height, breaking forces and maximum indentations depend on the adsorption strength and the bending rigidity of the virus. The radius of the AFM tip has a minor influence on the measured slope, associated with changes in the contact area. We have also shown that sudden drops in the force are not always a signature of breaking of the shell. Adsorption, faceting and buckling can also lead to indistinguishable force drops, evidencing that caution has to be taken in the interpretation of experiments. Finally, we have found that viruses show an anisotropic elastic response where the relative magnitude of the spring constants not only depend on the triangulation number, but also on the shape of the shell. Although in this work we have focused on the $T = 7$ structure, the Virtual AFM can be a useful tool for many future studies of indentation, buckling and breaking of different T-number viruses.

Acknowledgments

We thank Pedro J de Pablo and Antoni Luque for fruitful discussions. This work has been funded by the Spanish *Ministerio de Economía y Competitividad* through Grants No. FIS2008-01299, FIS2011-22603, and FIS2015-67837-P (MINECO/FEDER, UE), and the Spanish Network of Excellence in Physical Virology (FIS2015-71108-REDT).

ORCID iDs

David Reguera https://orcid.org/0000-0001-6395-6112

References

[1] Flint S J, Enquist L W, Racaniello V R and Skalka A M 2003 *Principles of Virology: Molecular Biology, Pathogenesis and Control of Animal Viruses* (Washington, DC: ASM Press)
[2] Gelbart W M and Knobler C 2009 Pressurized viruses *Science* **323** 1682–3
[3] Kindt J, Ben-Shaul A, Tzlil S and Gelbart W M 2001 DNA packaging and ejection forces in bacteriophage *Proc. Natl Acad. Sci. USA* **98** 13671–4
[4] Cordova A, Deserno M, Gelbart W M and Ben-Shaul A 2003 Osmotic shock and the strength of viral capsids *Biophys. J.* **85** 70–4
[5] Purohit P K, Inamdar M M, Grayson P D, Squires T M, Kondev J and Phillips R 2005 Forces during bacteriophage DNA packaging and ejection *Biophys. J.* **88** 851–66
[6] Evilevitch A, Lavelle L, Knobler C M, Raspaud E and Gelbart W M 2003 Osmotic pressure inhibition of DNA ejection from phage *Proc. Natl Acad. Sci. USA* **100** 9292–5
[7] Smith D E, Tans S J, Smith S B, Grimes S, Anderson D L and Bustamante C 2001 The bacteriophage ϕ29 portal motor can package DNA against a large internal force *Nature* **413** 748–52
[8] Le Romancer M, Gaillard M, Geslin C and Prieur D 2007 Viruses in extreme environments *Rev. Environ. Sci. Biotechnol.* **6** 17–31
[9] Hernando-Perez M, Miranda R, Aznar M, Carrascosa J L, Schaap I A T, Reguera D and de Pablo P J 2012 Direct measurement of phage ϕ29 stiffness provides evidence of internal pressure *Small* **8** 2365–9
[10] Michel J P, Ivanovska I L, Gibbons M M, Klug W S, Knobler C M, Wuite G J L and Schmidt C F 2006 Nanoindentation studies of full and empty viral capsids and the effects of capsid protein mutations on elasticity and strength *Proc. Natl Acad. Sci. USA* **103** 6184–9
[11] Klug W S, Bruinsma R F, Michel J-P and Knobler C M 2006 Failure of viral shells *Phys. Rev. Lett.* **97** 228101
[12] de Pablo P J and Mateu M G 2013 *Structure and Physics of Viruses* vol 68, ed M G Mateu (Dordrecht: Springer) ch 18, p 519
[13] Ivanovska I L, de Pablo P J, Ibarra B, Sgalari G, MacKintosh F C, Carrascosa J L, Schmidt C F and Wuite G J L 2004 Bacteriophage capsids: tough nanoshells with complex elastic properties *Proc. Natl Acad. Sci. USA* **101** 7600–5
[14] Mateu M G 2012 Mechanical properties of viruses analyzed by atomic force microscopy: a virological perspective *Virus Res.* **168** 1–22
[15] de Pablo P J 2013 *Structure and Physics of Viruses* vol 68, ed M G Mateu (Dordrecht: Springer) ch 8, p 247
[16] Marchetti M, Wuite G and Roos W 2016 Atomic force microscopy observation and characterization of single virions and virus-like particles by nano-indentation *Curr. Opin. Virol.* **18** 82–8
[17] Roos W H, Bruinsma R and Wuite G J L 2010 Physical virology *Nat. Phys.* **6** 733–43
[18] Ivanovska I L, Miranda R, Carrascosa J L, Wuite G J L and Schmidt C F 2011 Discrete fracture patterns of virus shells reveal mechanical building blocks *Proc. Natl Acad. Sci. USA* **108** 12611–6
[19] Ortega-Esteban A, Pérez-Berná A J, Menéndez-Conejero R, Flint S J, Martín C S and de Pablo P J 2013 Monitoring dynamics of human adenovirus disassembly induced by mechanical fatigue *Sci. Rep.* **3** 1434
[20] Roos W H *et al* 2010 Squeezing protein shells: how continuum elastic models, molecular dynamics simulations, and experiments coalesce at the nanoscale *Biophys. J.* **99** 1175–81
[21] Llauró A, Luque D, Edwards E, Trus B L, Avera J, Reguera D, Douglas T, de Pablo P J and Castón J R 2016 Cargo-shell and cargo–cargo couplings govern the mechanics of artificially loaded virus-derived cages *Nanoscale* **8** 9328–36
[22] Carrasco C, Carreira A, Schaap I A T, Serena P A, Gómez-Herrero J, Mateu M G and de Pablo P J 2006 DNA-mediated anisotropic mechanical reinforcement of a virus *Proc. Natl Acad. Sci. USA* **103** 13706–11
[23] Ivanovska I, Wuite G, Jnsson B and Evilevitch A 2007 Internal DNA pressure modifies stability of WT phage *Proc. Natl Acad. Sci. USA* **104** 9603–8
[24] Ortega-Esteban A, Condezo G, Perez-Berná A J, Chillón M, Flint S J, Reguera D, San Martín C and de Pablo P J 2015 Mechanics of viral chromatin reveals the pressurization of human adenovirus *ACS Nano* **9** 10826–33

[25] Liashkovich I, Hafezi W, Kuhn J E, Oberleithner H, Kramer A and Shahin V 2008 Exceptional mechanical and structural stability of HSV-1 unveiled with fluid atomic force microscopy *J. Cell Sci.* **121** 2287–92

[26] Roos W H, Radtke K, Kniesmeijer E, Geertsema H, Sodeik B and Wuite G J L 2009 Scaffold expulsion and genome packaging trigger stabilization of herpes simplex virus capsids *Proc. Natl Acad. Sci. USA* **106** 9673–8

[27] Kol N *et al* 2006 Mechanical properties of murine leukemia virus particles: effect of maturation *Biophys. J.* **91** 767–74

[28] Kol N *et al* 2007 A stiffness switch in human immunodeficiency virus *Biophys. J.* **92** 1777–83

[29] Roos W, Gertsman I, May E, Brooks C L, Johnson J E and Wuite G J L 2012 Mechanics of bacteriophage maturation *Proc. Natl Acad. Sci. USA* **109** 2342–7

[30] Hernando-Pérez M, Pascual E, Aznar M, Ionel A, Castón J R, Luque A, Carrascosa J L, Reguera D and de Pablo P J 2014 The interplay between mechanics and stability of viral cages *Nanoscale* **6** 2702–9

[31] Sader J E, Chon J W M and Mulvaney P 1999 Calibration of rectangular atomic force microscope cantilevers *Rev. Sci. Instrum.* **70** 3967–9

[32] Gibbons M M and Klug W S 2007 Mechanical modeling of viral capsids *J. Mater. Sci.* **42** 8995–9004

[33] Landau L D and Lifshitz E M 1975 *Theory of Elasticity* (London: Pergamon)

[34] Vella D, Ajdari A, Vaziri A and Boudaoud A 2012 The indentation of pressurized elastic shells: from polymeric capsules to yeast cells *J. R. Soc. Interface* **9** 44855

[35] Buenemann M and Lenz P 2007 Mechanical limits of viral capsids *Proc. Natl Acad. Sci. USA* **104** 9925–30

[36] Ahadi A, Colomo J and Evilevitch A 2009 Three-dimensional simulation of nanoindentation response of viral capsids. Shape and size effects *J. Phys. Chem.* B **113** 3370–8

[37] Gibbons M M and Klug W S 2008 Influence of nonuniform geometry on nanoindentation of viral capsids *Biophys. J.* **95** 3640–9

[38] Aznar M, Luque A and Reguera D 2012 Relevance of capsid structure in the buckling and maturation of spherical viruses *Phys. Biol.* **9** 36003

[39] Vliegenthart G A and Gompper G 2006 Mechanical deformation of spherical viruses with icosahedral symmetry *Biophys. J.* **91** 834–41

[40] Buenemann M and Lenz P 2008 Elastic properties and mechanical stability of chiral and filled viral capsids *Phys. Rev.* E **78** 051924

[41] May E R, Feng J and Brooks C L III 2012 Exploring the symmetry and mechanism of virus capsid maturation via an ensemble of pathways *Biophys. J.* **102** 606–12

[42] May E R and Brooks C L III 2012 On the morphology of viral capsids: elastic properties and buckling transitions *J. Phys. Chem.* B **116** 8604–9

[43] Lidmar J, Mirny L and Nelson D R 2003 Virus shapes and buckling transitions in spherical shells *Phys. Rev.* E **68** 051910

[44] Nguyen T T, Bruinsma R F and Gelbart W M 2005 Elasticity theory and shape transitions of viral shells *Phys. Rev.* E **72** 051923

[45] Tama F and Brooks C L III 2005 Diversity and identity of mechanical properties of icosahedral viral capsids studied with elastic network normal mode analysis *J. Mol. Biol.* **345** 299–314

[46] Arkhipov A, Roos W H, Wuite G J L and Schulten K 2009 Elucidating the mechanism behind irreversible deformation of viral capsids *Biophys. J.* **97** 2061–9

[47] Zhmurov A, Rybnikov K, Kholodov Y and Barsegov V 2011 Generation of random numbers on graphics processors: forced indentation in silico of the bacteriophage HK97 *J. Phys. Chem.* B **115** 5278–88

[48] Kononova O, Snijder J, Brasch M, Cornelissen J, Dima R I, Marx K A, Wuite G J L, Roos W H and Barsegov V 2013 Structural transitions and energy landscape for cowpea chlorotic mottle virus capsid mechanics from nanomanipulation *in vitro* and in silico *Biophys. J.* **105** 1893–903

[49] Cieplak M and Robbins M O 2010 Nanoindentation of virus capsids in a molecular model *J. Chem. Phys.* **132** 15101

[50] Cieplak M and Robbins M O 2013 Nanoindentation of 35 virus capsids in a molecular model: relating mechanical properties to structure *PLoS One* **8** e63640

[51] Zink M and Grubmuller H 2009 Mechanical properties of the icosahedral shell of southern bean mosaic virus: a molecular dynamics study *Biophys. J.* **96** 1350–63

[52] Boyd K J, Bansal P, Feng J and May E R 2015 Stability of norwalk virus capsid protein interfaces evaluated by in silico nanoindentation *Front. Bioeng. Biotechnol.* **3** 1–8

[53] Aznar M and Reguera D 2016 Physical ingredients controlling stability and structural selection of empty viral capsids *J. Phys. Chem.* B **120** 6147–59

[54] Zandi R, Reguera D, Bruinsma R F, Gelbart W M and Rudnick J 2004 Origin of icosahedral symmetry in viruses *Proc. Natl Acad. Sci. USA* **101** 1555660

[55] Aznar M 2013 Coarse-grained modeling of the assembly and mechanical properties of viruses *PhD Thesis* Universitat de Barcelona

[56] Guerin T and Bruinsma R 2007 Theory of conformational transitions of viral shells *Phys. Rev.* E **76** 061911

[57] Morozov A Y and Bruinsma R F 2010 Assembly of viral capsids, buckling, and the Asaro–Grinfeld–Tiller instability *Phys. Rev.* E **81** 041925

[58] Siber A 2006 Buckling transition in icosahedral shells subjected to volume conservation constraint and pressure: relations to virus maturation *Phys. Rev.* E **73** 061915

[59] Widom M, Lidmar J and Nelson D 2007 Soft modes near the buckling transition of icosahedral shells *Phys. Rev.* E **76** 031911

[60] Mahalik J P, Brown K A, Cheng X and Fuentes-Cabrera M 2016 Theoretical study of the initial stages of self-assembly of a carboxysomes facet *ACS Nano* **10** 5751–8

[61] Katen S and Zlotnick A 2009 The thermodynamics of virus capsid assembly *Methods Enzymol.* **455** 395417

[62] Reddy V S, Giesing H A, Morton R T, Kumar A, Post C B, Brooks C L and Johnson J E 1998 Energetics of quasiequivalence: computational analysis of protein–protein interactions in icosahedral viruses *Biophys. J.* **74** 546558

[63] Caspar D and Klug A 1962 Physical principles in the construction of regular viruses *Cold Spring Harbor Symp. Quantum Biol.* **27** 1–24

[64] Carrillo-Tripp M, Shepherd C M, Borelli I A, Venkataraman S, Lander G, Natarajan P, Johnson J E, Iii C L B and Reddy V S 2009 VIPERdb 2: an enhanced and web API enabled relational database for structural virology *Nucl. Acids Res.* **37** 436–42

[65] Zeng C, Hernando-Pérez M, Dragnea B, Ma X, van der Schoot P and Zandi R 2017 Contact mechanics of a small icosahedral virus *Phys. Rev. Lett.* **119** 38102

[66] Agirrezabala X, Martin-Benito J, Caston J R, Miranda R, Valpuesta M and Carrascosa J L 2005 Maturation of phage T7 involves structural modification of both shell and inner core components *EMBO J.* **24** 3820–9

[67] Steven A C, Heymann J B, Cheng N, Trus B L and Conway J F 2005 Virus maturation: dynamics and mechanism of a stabilizing structural transition that leads to infectivity *Curr. Opin. Struct. Biol.* **15** 227–36

[68] Ionel A, Velázquez-Muriel J A, Luque D, Cuervo A, Castón J R, Valpuesta J M, Martín-Benito J and Carrascosa J L 2010 Molecular rearrangements involved in the capsid shell maturation of bacteriophage T7 *J. Biol. Chem.* **286** 234–42